SLOVAK UNIVERSITY OF TECHNOLOGY IN BRATISLAVA
FACULTY OF ELECTRICAL ENGINEERING AND INFORMATION TECHNOLOGY
INSTITUTE OF NUCLEAR AND PHYSICAL ENGINEERING

Ing. Andrej Novák

Dissertation thesis abstract

ENHANCED RADIATION-HARD SEMICONDUCTOR SENSORS FOR TIMEPIX AND TIMEPIX3 PIXEL DETECTORS

To obtain the academic title of:	Philosophiae doctor, PhD.
In the doctorate degree study programme:	Physical engineering
In the field of study:	Electrical and electronics engineering
Form of study:	Full-time
Place and date:	Bratislava, May 2024

SLOVAK UNIVERSITY OF TECHNOLOGY IN BRATISLAVA
FACULTY OF ELECTRICAL ENGINEERING AND INFORMATION TECHNOLOGY
INSTITUTE OF NUCLEAR AND PHYSICAL ENGINEERING

Dissertation thesis has been prepared at: Slovak University of Technology in Bratislava
Faculty of Electrical Engineering and Information Technology
Institute of Nuclear and Physical Engineering
Ilkovičova 3, 841 04 Bratislava

Submitter: Ing. Andrej Novák
Slovak University of Technology in Bratislava
Faculty of Electrical Engineering and Information Technology
Institute of Nuclear and Physical Engineering
Ilkovičova 3, 841 04 Bratislava

Supervisor: doc. Ing. Andrea Šagátová, PhD.
Slovak University of Technology in Bratislava
Faculty of Electrical Engineering and Information Technology
Institute of Nuclear and Physical Engineering
Ilkovičova 3, 841 04 Bratislava

Readers: doc. RNDr. Ivan Sýkora, PhD.
Comenius University Bratislava
Faculty of Mathematics, Physics and Informatics
Department of Nuclear Physics and Biophysics
Mlynská dolina, 842 48 Bratislava

doc. Dr. RNDr. Petr Alexa
VSB – Technical University of Ostrava
Faculty of Electrical Engineering and Computer Science
Department of Physics
30. dubna 22, 701 03 Ostrava

Dissertation thesis abstract was sent: ....

Dissertation thesis defence will be held on: .... at ....
Slovak University of Technology in Bratislava
Faculty of Electrical Engineering and Information Technology
Institute of Nuclear and Physical Engineering
Ilkovičova 3, 841 04 Bratislava

prof. Ing. Vladimír Kutiš, PhD.
Dean of FEEIT SUT in Bratislava

Contents

1 Motivation

Hybrid pixel detectors became part of many fields of physics and a wide range of applications [1]. Today, they can be found in medical imaging [2], dosimetry [3], neutron imaging, X-ray and gamma imaging, material research, conventional and FLASH radiotherapy [4, 5] accelerator beam instrumentation, or satellites orbiting the Earth [6]. These environments are characterised by high-intensity radiation fields that degrade and damage the detectors exposed for an extended period of time.

Hybrid pixel detectors are made up of three main parts that can be manufactured separately: sensor, chip, and readout interface. The detector sensor is made of semiconducting material, usually silicon (Si) or cadmium telluride (CdTe). Silicon is a well-known and widely used material; however, it has a low proton number (low density), leading to low detection efficiency and low stopping power compared to those of high-Z materials. Therefore, other high-Z materials are currently being investigated, such as CdTe or gallium arsenide (GaAs) [7, 8], which can be prepared as semi-insulating [9–11] or doped with chromium [12]. Another perspective radiation-hard semiconductor material used for the Timepix sensor is silicon carbide (SiC) [13] that is the main focus of this thesis.

One of the current state-of-the-art hybrid pixel detector is developed by the Medipix Collaboration named Medipix and Timepix. The Medipix/Timepix detectors are usually segmented into a 256×256 pixel matrix (65536 pixels in total) with an active area of 1.4×1.4 mm^2 where each pixel has a pitch of 55 microns and accommodates electronics for individual signal analysis [14]. The great advantage of hybrid pixel detectors is the possibility of distinguishing the composition of detected radiation field on the basis of the morphology and spectral information of the detected events. This is demonstrated through the thesis using different laboratory isotopes, proton cyclotrons (proton energy range 8 - 225 MeV), electron cyclotrons (electron energy range 5 - 8 MeV) and fast-neutrons (neutron energy range 0.3 - 17.5 MeV) in combination with Timepix/2/3 detectors equipped with Si, CdTe, GaAs:Cr, SI-GaAs and 4H-SiC sensors of different thicknesses and applied bias voltages.

For the purpose of preliminary pre-processing of the acquired Timepix data, Data Processing Engine (DPE) software tool was used [15]. The DPE performs the per-pixel calibration and calculation of multiple morphological and spectral parameters of the resolved clusters. The output of DPE is a raw set of data that must be further analysed and for this purpose I have developed a library of different Python methods and classes that offer tools for thorough analysis and complex parameter cluster filtration. These optimised methods can be further scaled and adjusted to fit any specific purpose.

2 Dissertation thesis objectives

The main objectives of this dissertation thesis are as follows:

- Evaluation of newly developed semiconductor sensors for Timepix and Timepix3 hybrid pixel detectors based on perspective semiconductor materials such as SI-GaAs, GaAs:Cr, 4H-SiC, CdTe.
- Experimental comparison of detection response and physics products of the Timepix detectors with newly developed sensors with existing sensors, in particular silicon.
- Analysis and processing of experimental data acquired at various radiation sources, including electron and proton beams from particle accelerators as well as at neutron sources.
- Creation of a methodic approach for data filtration and processing for mixed-radiation field measurements and particle group type separation into individual radiation fields.

3 Current semiconductor materials for Timepix detectors

For the hybrid pixel detector sensor, the most common choice of the semiconducting material is Si or CdTe. These are manufactured in a variety of thicknesses ranging from 100 μm to 5000 μm (in case of CdTe [16]). Sensor parameter requirements vary depending on the setup of the experiment and the type of measurement. In the field of computed tomography, a high probability of photon interaction with sensor material in the range of up to hundreds of keV is desirable, since this is the maximum energy of most computed tomography machines. The probability of an X-ray photon interaction with a Si sensor drops rapidly around 15 keV compared to high-Z materials such as CdTe or GaAs.

The key requirement regarding sensor materials is their radiation resistance, since these detectors are primarily used in intense-radiation areas and facilities like synchrotrons, electron microscopes, particle accelerators or in space applications where they are subjected to space weather and high-energy ionising particles. Radiation resistance is an advantage of the GaAs and SiC sensors. Semiconductor materials closely investigated in this thesis and their characteristic parameters are shown in Table 1.

Property	Unit	Si	4H-SiC	GaAs	CdTe
Density	[g.cm^{-3}]	2.328	3.21	5.32	5.85
Dielectric constant	[-]	11.7	9.66	12.8	10.2
Band gap	[eV]	1.12	3.23	1.424	1.44
Ionization energy	[eV]	3.62	7.28	4.8	4.7
Fano factor	[-]	0.115	0.128	0.12	0.12
Intrinsic carrier concentration	[cm^{-3}]	1×10^{10}	-	2.1×10^{6}	-
Intrinsic resistivity	[Ω.cm]	3.2×10^{5}	1×10^{5}	3.3×10^{8}	1×10^{8}
Electron mobility	[cm^2/V/s]	≤ 1400	≤ 900	≤ 8500	≤ 700
Hole mobility	[cm^2/V/s]	≤ 450	≤ 120	≤ 400	≤ 65

Table 1: Comparison of a selected properties of commonly used semiconductor materials at room temperature [17].

Silicon (Z = 14) is the material most commonly used as a semiconductor detector. Its manufacture is a well-known process, as it has been used in processor production and integrated circuits since the 1960s. Among all semiconductor materials, they are cheap and provide good homogeneity and moderate values regarding the intrinsic resistivity and charge carrier resistivity. Silicon is suitable for X-ray/gamma imaging up to 20 keV energies; however, above this energy, silicon has a large drop in probability of photon interaction with detection media, and therefore high-Z materials are desirable for X and gamma imaging. Silicon sensors for Medipix/Timepix detectors are usually manufactured as 100 μm, 300 μm, or 500 μm thick. The larger thicknesses are better for X and gamma imaging, whereas the smaller thicknesses are suitable for ion imaging. The most commonly used silicon thickness is 300 μm, and it has been used for all kinds of experiments, from X-ray imaging, neutron imaging, in the International Space Station, satellites monitoring the radiation fields [6], etc. It is an appropriate sensor for general use.

Intrinsic carrier concentration is a property that influences the signal-to-noise ratio, a parameter that must be high for sensor materials used at room temperatures. In this sense, the sensor materials CdZnTe (Z = 48/30/52), CdTe (Z = 48/52) and GaAs (Z = 31/33) are also suitable for room-temperature operation while simultaneously providing a high probability of photon interaction, making them suitable for computed tomography or other X or gamma imaging [18]. Germanium is a high-quality material with similar advantages as other high-Z materials; however, it has a low band gap on the order of 0.661 eV, which causes a high noise current at room temperature and requires constant cooling, which makes it unsuitable for use in hybrid pixel detectors. These high-Z materials also provide a high stopping power, characteristics that mean that charged particles are more effectively stopped in the sensor material compared to those of the low Z material such as Si. High-Z materials are suitable for direct detection of heavy charged particles in accelerator facilities or recoil or secondary charged particles, for example, in proton therapy and determination of correct dose delivery.

Both CdZnTe and CdTe sensor array and pixel detectors have been developed since the end of 1990s. Most manufacturers offer this hihg-Z alternative for Si sensors. The CdTe sensors are usually manufactured in 1 mm or 2 mm thick versions. The high proton number combined with high thickness is advantageous in almost any type of experiment or measurement. At high particle fluxes, CdTe suffers from high polarisation, which leads to requirements of higher measurement time (frame acquisition time must be set low, introducing a higher number of frame dead time, and turned off after a short measurement to achieve sensor depolarisation), leading to time-consuming measurements. The CdTe manufacturing process allows us to produce sensors with good homogeneity even at high thicknesses with the proposition of a 5 mm thick sensor [16]. At such thicknesses, it is suitable for detection of high-energy charged particles that may be fully stopped in its volume.

Investigating GaAs for sensor material has begun around the same time as CdTe [19] and provided a proof of concept that GaAs is suitable for hybrid pixel detectors [20]. The undoped SI-GaAs sensor has also been investigated and developed by a joint collaboration of the Slovak Academy of Sciences in Bratislava and the Slovak University of Technology in Bratislava [9, 10, 21, 22]. The SI-GaAs suffers from a number of electrophysical limitations. To improve its characteristics, chromium impurities are doped into the bulk to compensate for the EL2 impurity centres. This leads to the absence of current oscillations and decreases the cross-section of electron capture. With chromium impurities in GaAs it is possible to achieve a uniform high electric field distribution throughout the whole sensor. The improved GaAs:Cr sensor can be manufactured in thicknesses up to 1 mm [23–25]. The advantage of SI-GaAs compared to chromium-doped GaAs is its improved energy resolution comparable with Si. The back current is lower thanks to the Schottky contact and also provides an improved thermal stability. The possible applicable bias voltage is higher leading to higher electric field and faster charge carrier collection. The charge sharing is also lower in SI than chromium doped.

Silicon carbide is a material that has been steadily investigated for radiation detection and has been shown to be a suitable detector for use in high-temperature and high-radiation conditions where common sensors cannot perform adequately [13, 26, 27]. The SiC is suitable for harsh conditions. Its large band-gap energy leads to low leakage current even at high biases, a property that is required for low-noise operation and high-energy resolution. The energy required for electron-hole creation is small enough to ensure a high signal-to-noise ratio. The dielectric constant is the lowest among the materials stated in Table 1, this parameter allows for operation with low capacitance and therefore reduces the white noise of the front-end electronics leading to better energy resolution. The epitaxial grown single crystal has high purity, homogeneity, and no defects; however, it is manufactured at a higher cost. The lack of impurities ensures full charge collection, low leakage current, and high energy resolution. Silicon carbide has a high atomic displacement energy E_d, a characteristic that is related to the creation of defects, e.g., by long term exposition to radiation during detector operation, that lead to deterioration in energy resolution and charge trapping that affect charge collection in the sensor volume. The atomic displacement energy E_d for diamond is $E_{dC} \approx 40$ eV and for SiC $E_{dSi} = 35$ eV and $E_{dC} = 22$ eV. The high thermal conductivity of SiC allows one to effectively cool down and maintain its operating temperature even during thermally demanding experiments with long exposures to high radiation [28, 29]. Currently, two fully functional SiC sensors are being investigated that were prepared, tested and bump-bonded to the Timepix3 chip with a MiniPIX application-specific integrated circuit (ASIC) [30].

4 Instruments: New sensors for Timepix detectors

Gallium arsenide sensors are denoted as high-Z sensors for their proton number (Z = 31/33) that is higher than that of Si (Z = 14) which is commercially available and well known. This feature of GaAs has many advantages in the field of radiation detection from increased high-energy photon detection, to high stopping power of electrons and light and heavy ions. The GaAs offers small fluorescence probability, high stability, high electron mobility of 8500 $cm^2/V/s$, and therefore fast charge collection, that is required for time-of-flight experiments and measurements requiring fast detection. Another advantage is its high maximal electron drift velocity of 2×10^7 cm/s.

The decades-long collaboration of SAS and FEEIT SUT yielded multiple results achieved on the SI-GaAs that finally led to manufacture of SI-GaAs sensor for Timepix detector [21], see Figure 1 (left). Crystal for the SI-GaAs was grown using vertical gradient freeze and 350 μm thick wafer was cut. The sensor was segmented into a matrix of 256×256 pixels with a size of 55 μm × 55 μm and bump-bonded at AdvaFab to the Timepix chip. The bump-bonded Timepix chip was connected to a FitPIX readout that can be connected to a personal computer and controlled using the Pixet software developed at Advacam. A bias scan was performed that showed a degradation of performance after reaching 60 V that was based on cross-talk between neighbouring pixels that is induced by high electric field interference. In [10, 11] the performance of SI-GaAs is discussed in greater detail including the energy resolution that was 4.4 keV full width at half-maximum (FWHM) using the 59.6 keV peak of the ^{241}Am laboratory

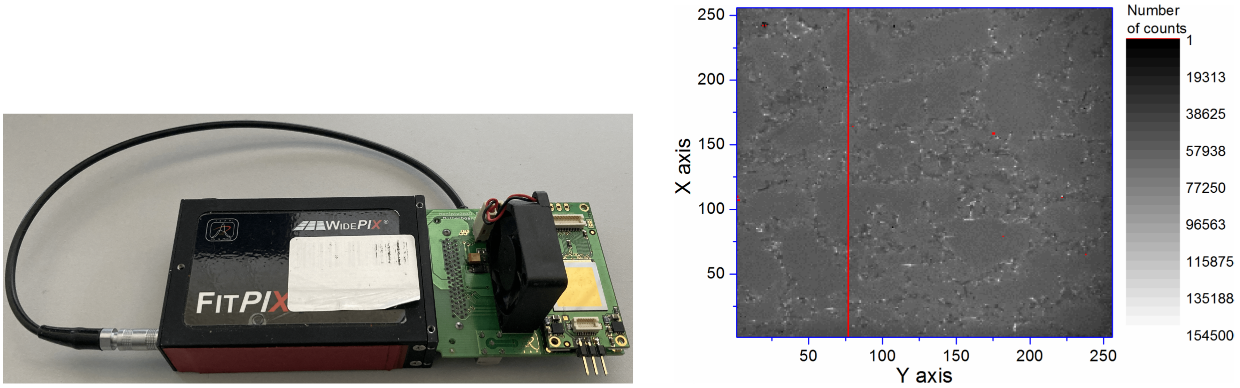

Figure 1: The SI-GaAs sensor bump-bonded to Timepix chip shown in the full assembly with FitPIX readout electronics (left). Open-beam image (right) obtained using X-ray tube and SI-GaAs 350 μm sensor operated at 60 V bias. The red line represents defective column of masked pixels.

isotope.

The motivation of the development of SiC sensors lies in a number of parameters important for exposure mainly in a radiation harsh environment. The SiC sensor has a high breakdown voltage (4×10^6 V cm^{-1}, allowing for high applicable bias), high electron mobility (circa 900 cm^{2}V^{-1}s^{-1}, advantage for time-of-flight experiments), as in GaAs the SiC has a high electron saturation drift velocity (2×10^7 cm^{-1}), 3.23 eV band gap energy, and large displacement energy E_d that as a result leads to its increased radiation hardness. Detector with these qualities is well suited for applications with high radiation dose such as beam monitoring at accelerator facilities, hadron therapy experiments, synchrotron imaging applications, and space applications from dosimetry to space weather monitoring.

For the investigation of SiC as a sensor material for the Timepix3 chip, two companies, CREE Wolfspeed (USA, F04-W0048 and D02-W0048) and LPE Epitaxial Technology (IT, L06-W0048 and L07-W0048), prepared 4H-SiC for four sensors. Epitaxial growth of SiC was used to achieve 80 μm and 100 μm thick layer, respectively. Sensors were used in C-V measurements to determine their depth characteristics of bias depletion, depth capacitance measurement results shown in Figure 3. From these graphs, it is visible that the ideal bias is as high as possible up to 300 or 400 V. After bump-bonding of the sensors to the Timepix3 chip, the detectors were connected to the MiniPIX readout; see Figure 4 (right). The four detectors were tested with the following results. The first 100 μm thick sensor with SiC supplied by CREE (F04-W0048) had a high leakage current and its bias was not raising leading to the conclusion that the chip is shorted. The second sensor (D02-W0048) was operating up to 350 V where a breakdown occurred. With this sensor, X-ray irradiation was also performed with Cd. At operating bias of 200 V, the detector had a weak signal as a result of poor depletion, meaning that the sensor requires much higher bias for proper operation. However, the Timepix3 cannot withstand a bias higher than 300 V before causing a breakdown through the edge of the sensor.

The first sensor supplied by LPE (L07-W0048) had 369 bad pixels that were masked mainly around the edges of the sensor. Current-voltage measurement yielded a current of less than 0.5 μA from a 20 V to 200 V bias with a step of 20 V. The bias voltage test was performed with Fe XRF on 6.4 keV. Afterwards, the L07-W0048 was tested using X-ray tube with 50 kV and aimed for 23 keV Fe resolution through threshold scan. The left-hand corner is masked due to the noise. The 23 keV Fe peak was resolved at 41 DAC with a sigma value of 5.2. At 100 V bias 40 μm thickness is depleted while at 200 V bias 60 μm were achieved.

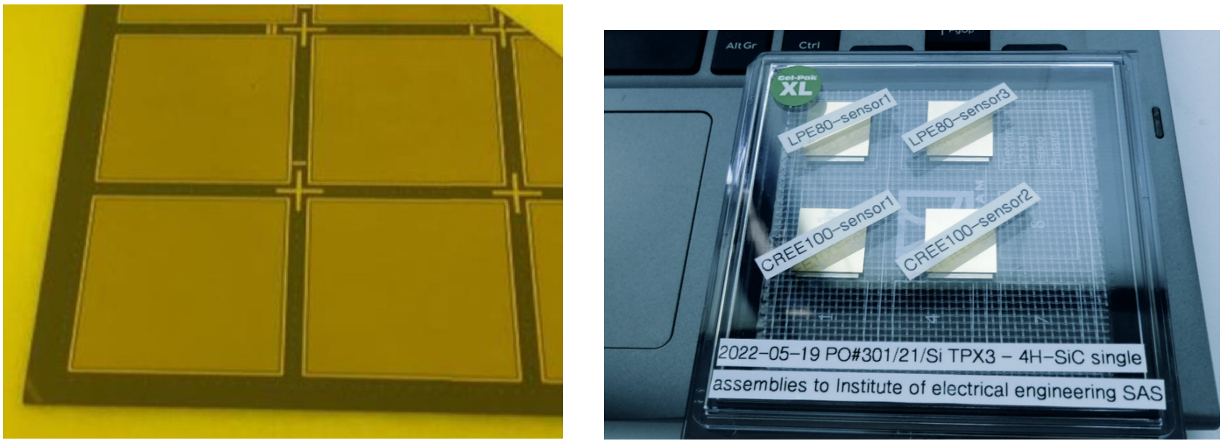

Figure 2: A photo of four 80 μm thick pixelated structures prepared on 4H-SiC epitaxial layer wafer and sensor assemblies for measurements and testing.

The second sensor (L06-W0048) was subjected to the same measurements as the L07-W0048 and performed significantly better. The number of pixels masked during the digital test was 10 and after the X-ray imaging, this number was raised to 68. It was able to operate with up to 260 V bias, and in the acquired spectrum both Cd peaks, 23 keV and 26 keV, were resolved together with the ^{241}Am 59.6 keV peak.

The sensors used in this work were limited to a bias of 200 V to prevent electrical shortages. However, due to the limited bias voltage, only 65 μm out of 80 μm detector sensor thickness could be fully depleted. On top of the 80 μm active layer (nitrogen doped layer, doping concentration $1{\times}10^{14}$ cm^{-3}) there is a buffer (concentration $1{\times}10^{18}$ cm^{-3}) and a bulk layer ($2{\times}10^{18}$ cm^{-3}) which together with the non-depleted epitaxial region form a dead layer of 365.5 μm thick that absorbs radiation; see Figure 4 (left). As a result, low-energy X-ray imaging requires an extended exposure time to acquire a significant number of counts (see Figure 5 where mouse paw was irradiated using SiC and 300 μm Si and indicates that a higher acquisition time is required to obtain a sufficient number of counts of low-energy photons). During the process of standard detector energy calibration using X-ray fluorescence [31], the exposure time has been adjusted to address these limitations. Alpha particle measurements using laboratory isotopes such as ^{241}Am (5.5 MeV) were not feasible, given that the particle range is in the order of microns and stops within the detector material. The sensor is suitable for the detection of accelerated high-energy light and heavy ions that can transverse to the active volume. An alternative approach for particle tracking and detection of accelerated particles is to tilt the sensor to enable the particle beam to impinge on the sensor from the side.

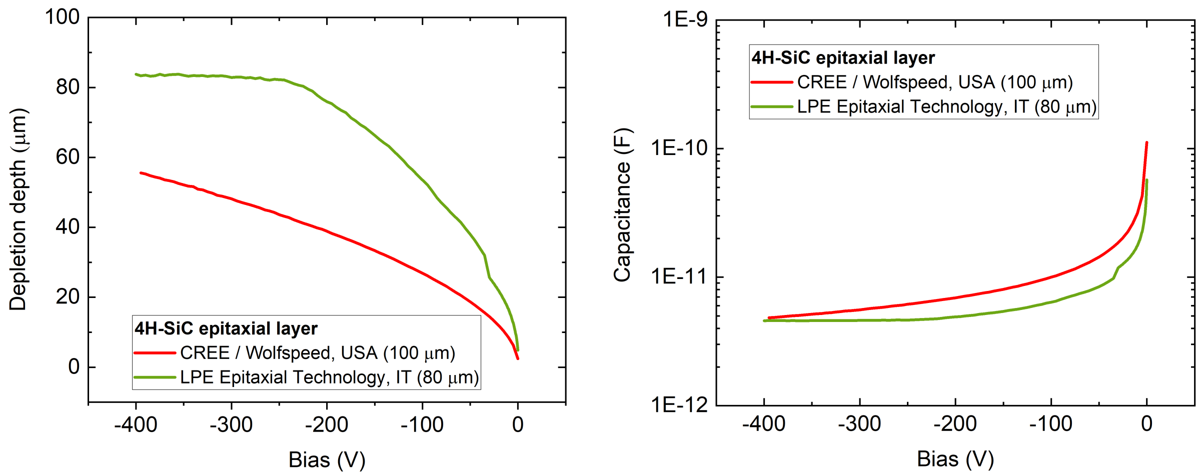

Figure 3: The depletion depth as a function of reverse bias voltage (left) and capacitance as a function of reverse bias voltage (right) in 4H-SiC sensor supplied by CREE Wolfspeed (red) and LPE Epitaxial Technology (green) [32].

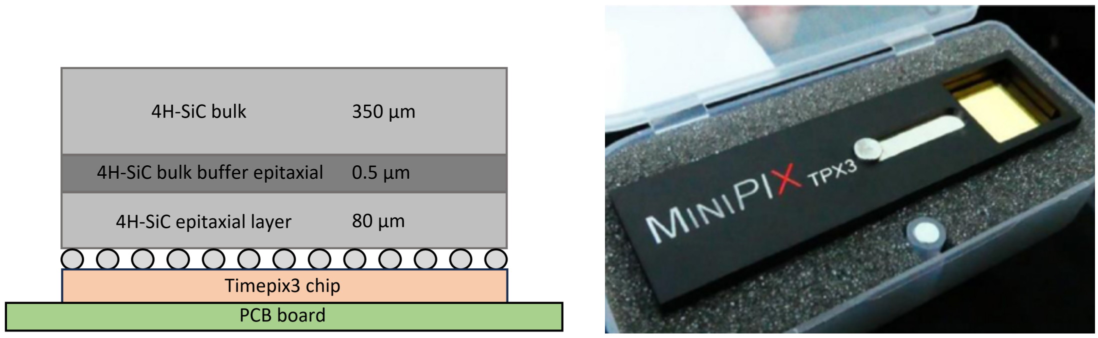

Figure 4: Diagram of the cross section of the SiC sensor (left) showing the bulk, buffer, and epitaxial grown layers. With 200 V applied bias voltage, the radiation sensitive volume is 65 μm thick facing down to the Timepix3 ASIC bump contacts. The remaining 365.5 μm thick volume facing up is regarded as a nonsensitive absorption layer. On the right, Timepix3 MiniPIX detector equipped with a SiC sensor is shown.

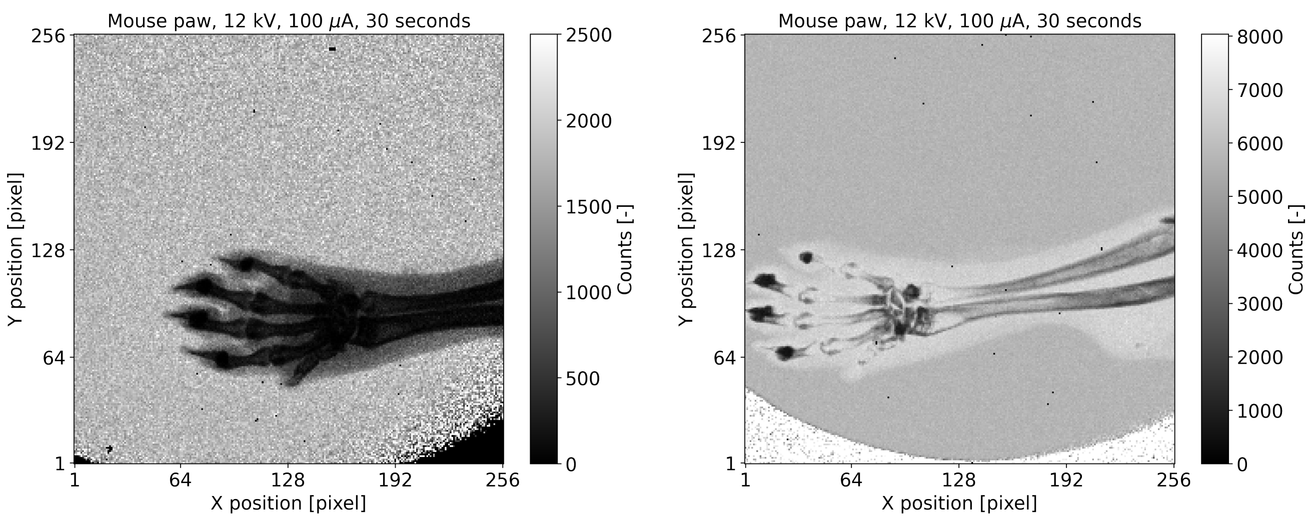

Figure 5: A mouse paw X-ray irradiation using X-ray tube with Ag anode operated at 12 kV and 100 μA. On the left is the 4H-SiC L06-W0048 sensor with 65 μm thickness while on the right is an image obtained using 300 μm Si sensor. Both images were acquired over 30 second X-ray sensor irradiation (300 frames, 0.1 s acquisition time). Both images are flat-field corrected.

5 Methods: Characterization of sensor response to radiation and data processing

Currently, new semiconducting 4H-SiC and SI-GaAs radiation-hard sensors are in production. In addition to the material characteristics of the sensors, the importance of full characterisation of their performance in imaging applications, spectral particle tracking, and temporal stability is required. The high granularity of the detector and the spectral response per-pixel can be used to examine and evaluate the uniformity and homogeneity of the radiation response and charge collection of the semiconductor sensor [33]. The response of the Timepix3 chip ASIC can be evaluated with respect to the sensor material, its thickness, bias voltage and, in the case of accelerated charged particles, such as electrons, protons, or heavy ions, also the angle of incidence.

The hybrid pixel detectors offer a high granularity of individual small solid-state detectors, pixels, that are ideal for time, position, and spectral tracking of charged particles. The calibration measurements with hybrid pixel detectors are usually performed at electron or heavy charged particle accelerators (particles with $A \geq 1$) that produce a well-defined, stable, and mono-energetic beam ideal for determination of detector's performance.

When an ionising particle impinges on the sensor or passes through it, it ionises the sensor volume and creates electron-hole pairs that are then collected by pixels. An ionising particle such as a proton in the range of tens of MeV creates a multipixel event in the Timepix3 detector, as it travels through the sensor volume. As a result of this interaction, a cluster of events is formed and detected. Using grouping algorithms [34], each particle interaction can be analysed at the microscale level. An illustration of high-resolution spectral tracking analysis is shown in Figure 6.

An analysis can be performed to correlate parameters such as total deposited energy, cluster size, height (maximum energy in a cluster), track length, and further morphology, spectral (energy loss), and tracking parameters with respect to sensor-related parameters such as applied bias or sensor material. This evaluation is also used to analyse and identify the radiation components of mixed radiation fields [35].

With increasing sensor thickness, the track length and particle deposited energy increase with its minimum in the thinnest sensor, 100 μm Si, and its maximum in 2000 μm thick CdTe. With an increase in the Z number of the semiconducting sensor material, the height of the cluster and the energy deposited per-pixel are higher in CdTe ($Z = 48/52$) and GaAs:Cr ($Z = 31/33$) than in Si ($Z = 14$). For linear energy transfer (LET) as a measure of energy loss along a track, the highest values are for CdTe and GaAs:Cr as a result of their high stopping power.

A number of parameters can be calculated for each cluster that is separated using the clustering algorithm and performing the per-pixel calibration. These parameters can be divided into basic cluster variables and advanced or derived cluster variables. The aim of derived cluster variables is to perform experiment-specific analysis of the acquired dataset, for example, coincidence analysis or specific interaction separation and observation of resulting processes. Some of the basic cluster variables which are individually calculated are sum of cluster deposited energy, maximum energy in cluster, cluster size, weighed centre coordinates, axis and polar angle, 2D length and 2D width, linearity, roundness, etc.

In many cases there is a need to process the data further either to mask pixels or detector region that became noisy during the data acquisition or perform additional task that arise from the nature of experiment, analysis, or visualisation. For this reason I developed a complex Python library that contains

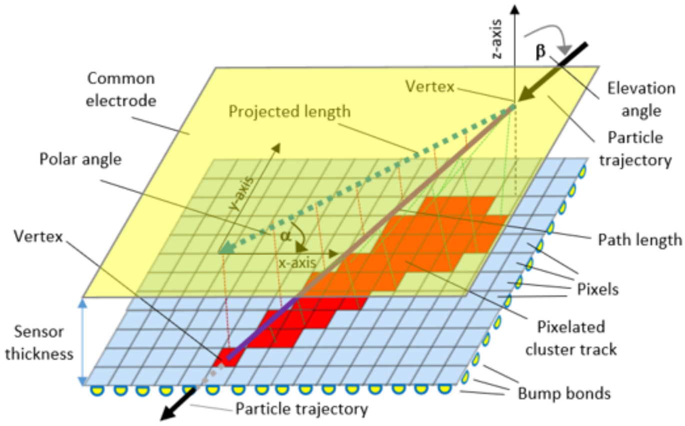

Figure 6: Illustration of high-resolution spectral tracking in Timepix3 detector of charged particles. The microscale morphology and pattern recognition analysis of the registered signal, a cluster of red pixels, enables to derive the path length in 3D (purple line) across the radiation sensitive volume with its entrance and exit points (labelled as vertices), the 2D projected length (dashed green line) on the plane of the sensor, the polar angle α and an elevation or zenith angle β of the particle trajectory [34].

functions for operations with preprocessed data operation from data selection and manipulation, cluster analysis, skeletonization, visualisation, performing dataset and cluster filtration on the pre-selected criteria and much more. All developed functions are optimised for fast execution, no unnecessary code repeatability, and the lowest achievable memory use. These optimisations were vital since the usual datasets used for the analyses can be up to gigabytes in size. These datasets can also require a specific approach to their processing due to the limiting capabilities of available computing power and memory when the whole dataset cannot be loaded directly and requires a specific approach consisting of continuous data loading in chunks, memory data rewriting, and consecutive optimal storing of the results. Through this thesis all the results were generated using this library with specific tweaks and adjustments for each individual experiment, measurement, analysis, or detector. These adjustments are always based on the insights made via knowledge of nuclear physics, different types of radiation, and their characteristic behaviour in sensor material interaction.

An important additional parameter that was developed for the purpose of this thesis and particle filtration was a cluster skeletonisation process. The process consists of multiple iterations where the peripheral pixels of the cluster are removed in an erosion process with the only exception of the cluster end/entry pixels. Using the Skeletonise module of the Sci-kit Image Python library [36], it is possible to acquire a skeleton of each particle cluster track. In this process, the cluster border pixels are first identified and eroded under the single condition that the particle skeleton connectivity is not broken by this removal. The process iterates until only the skeleton pixels are left.

Cluster skeleton analysis based on the skeleton branching, number of joint, and end points can be further utilised for a filtration of rare events and anomaly detection such as delta ray generation or fragmentation events with selected number of fragments. On top of that, each fragment path of the skeleton can then be separated from the total cluster and analysed individually, giving a further insight into a parameters of selected fragment and its own physical or morphological characteristics. Separation of individual skeleton parts can be achieved by employing a walking pixel algorithm that traces its path between end and joint points. An example of detected fragmentation is shown in Figure 7 where a 150 MeV proton impinges on a 500 μm sensor at a 75° elevation angle and together with a joint region

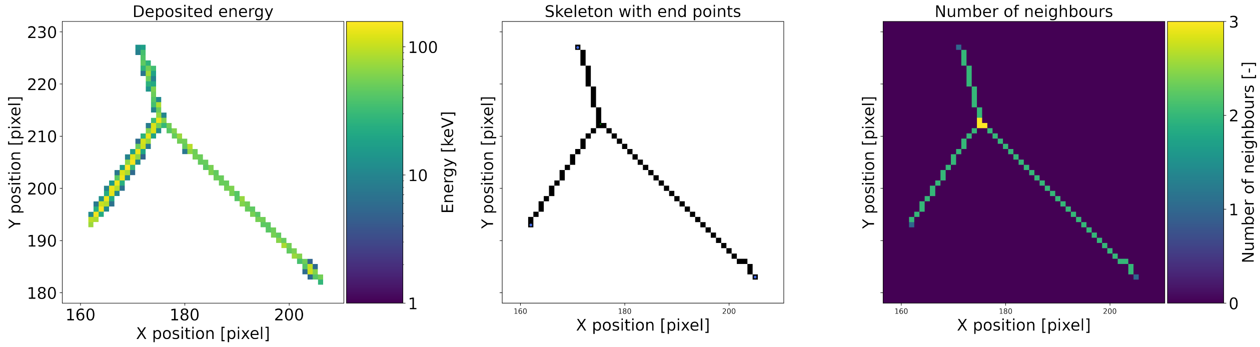

Figure 7: An example of rare detected event filtered based on the number of resolved skeleton ends.

the cluster track has three end points indicating that track branching has occurred.

On the basis of the type of radiation that interacts with the sensor material and its energy upon sensor impinging, a different response can be observed. The differences between radiation types are visible on the basis of both morphological and spectral parameters of the clustered event. The photons interaction is very localised and in the sensor it can usually be resolved as one- to four-pixel events. In most cases, the electron cluster events can be recognised by their curving as the electron traverses through the sensor and recoils off of electrons of sensor lattice atoms and high divergence along its cluster axis. In case of light ions, their path is narrow through the sensor and their range is energy dependent with the Bragg curve characteristics. Heavy ions that impinge on the sensor do not have a long range due because of their high charge and high ionisation potential, but have a lower range when compared to light ions.

In the case of light ions or electrons with divergent path it can be desirable to analyse their profile. Therefore, before acquiring its profile, a narrowing of the cluster track has to be performed. It can be described as a simple process that is achieved by calculating the cluster centroid and centroid of each individual row or column (based on the cluster orientation) and performing a row/column shift by the difference between the two. This way the original information stored in the pixels is preserved, and only their position is updated.

6 Achieved results and discussion

6.1 Response to energetic protons in 8 - 226 MeV energy range

Each sensor exhibits its own characteristic response to the detection of ionising particles. The CdTe and GaAs:Cr are both high-Z sensors with a high stopping power and a distinct charge-sharing extent. Therefore, these sensor characteristics lead to their specific spectral response to different particles such as protons. Furthermore, the sensor thickness and the applied bias influence the spectral response of each sensor. The direction of the incoming particles relative to the sensor surface plane determines the characteristic morphology and spectrometry of the pixelated clusters. The same particle deposits less energy in the thinner volume on a smaller surface compared to a thicker volume. Silicon and GaAs:Cr sensors with the same thickness of 500 μm achieve similar results with respect to cluster size; however, the high stopping power of the GaAs:Cr sensor shows up in the deposited energy per-pixel. As expected, the longest tracks are detected in the thickest sensor, 2000 μm CdTe, which produces tracks with a large low-energy halo and characteristic charge cloud at the end of the track, where the attenuated proton

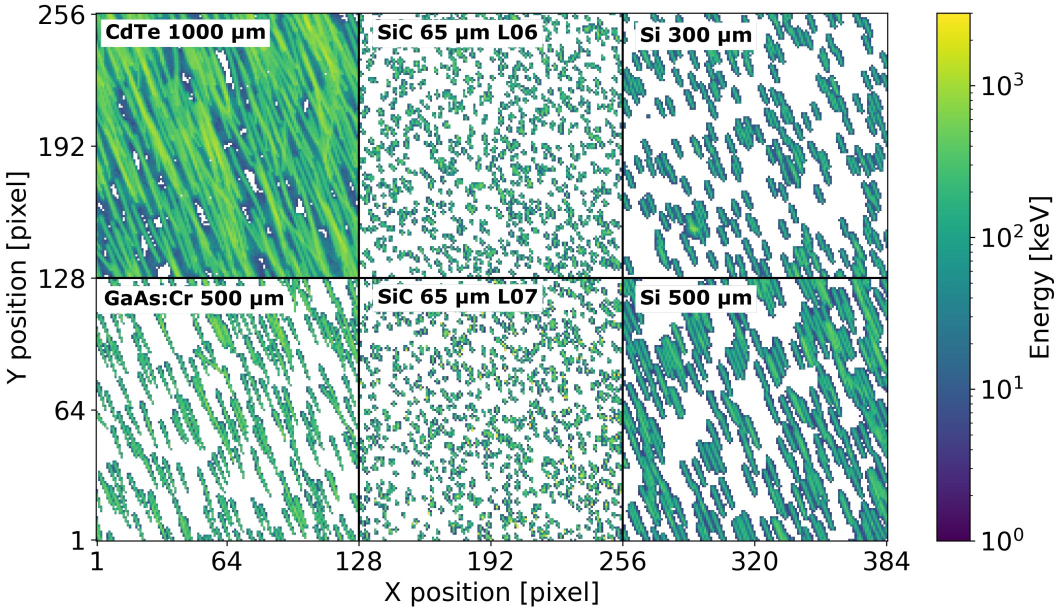

Figure 8: The deposited energy by 1000 events with size larger than three pixels in sensors used at an experiment at U120-M cyclotron with 31 MeV proton beam energy and 60° angle of beam incidence. A region with 128×128 pixel dimension was selected from each sensor.

is fully absorbed and locally deposits all of its remaining energy. An illustrative matrix of the energy deposited by 1000 events with size larger than three pixels during 31 MeV irradiation at 60° incidence angle detected by each detector is shown in Figure 8.

To fully describe all sensors, an analysis was performed based on the distribution of energy in the cluster, the height of the cluster (maximum per-pixel energy in the cluster), the size of the cluster and LET. Two distributions of the cluster deposited energy and LET of filtered proton clusters are shown in Figure 9 for five detectors at a proton beam energy of 31 MeV and a 50° irradiation angle. In the total energy distribution deposited in the cluster, the peaks are lined with CdTe at the maximum position, followed by the GaAs:Cr, and Si sensors aligned by their respective thicknesses from 500 μm to 100 μm. The cluster height distribution can be separated into two groups. The first cluster height group corresponds to high-Z sensors CdTe and GaAs:Cr while the second group is formed by three low-Z Si sensors. Before pre-processing and analysis, a thorough investigation of noisy pixels was conducted for all sensors. The difference in Z and therefore the stopping power of the sensor materials is visible in the LET distribution, where all the Si peaks are positioned close to the same value. An interesting observation can be made where the GaAs:Cr with a thickness of only one-quarter that of CdTe performs the same and even outperforms the CdTe sensor. Preliminary analysis of all cluster parameters from the acquired data is vital for decomposition of the mixed radiation field and subsequently filtration of its components.

The 4H-SiC sensors used during these measurements provide only a limited active volume. Here, the non-sensitive 365.5 μm thick layer acts as a dead zone or barrier for direct radiation detection. As a result, only a small portion of the impinging high-energy particle energy is deposited in the active sensor volume. In order to achieve full particle absorption, high angles of beam incidence are required close to the parallel position. In a fully depleted sensor without any material barrier above the active volume, different impinging radiation results in events with different morphological and spectral that are characteristic based on the radiation type as well as its energy with only a limited overlap [33]. In case of 4H-SiC sensors these characteristic boundaries between particle groups are less pronounced, leading

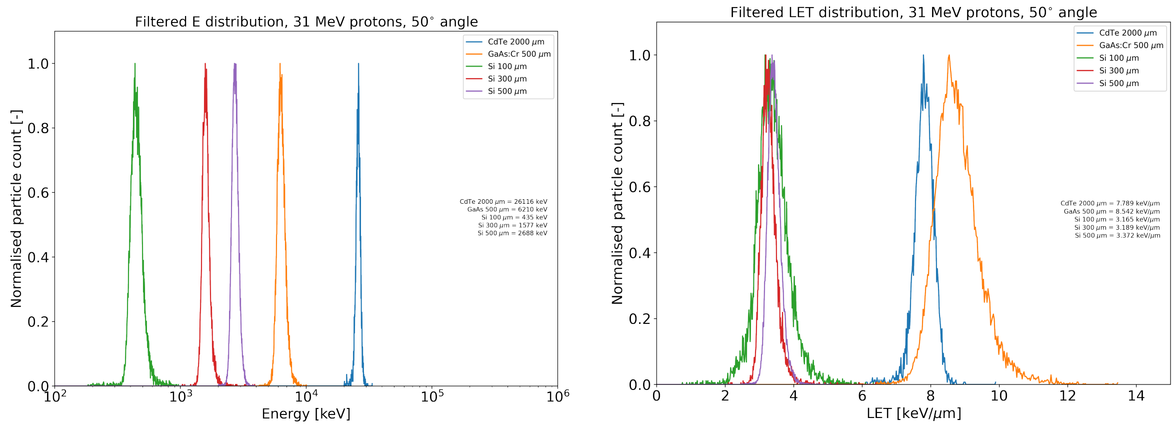

Figure 9: Distribution of the energy (left) and LET from the data acquired with 31 MeV proton beam at 50° angle of proton beam incidence for all sensors.

to a limited use of all morphological and spectral parameters. In the 4H-SiC only a few parameters were used for high-energy particle filtration, and mainly the cluster deposited energy and cluster size were proven to be the most effective while simultaneously achieving a high ratio of filtered proton tracks to unwanted or background events. As the angle increases, the length of proton tracks in the active volume increases, which leads to a higher deposited energy. At high angles, a shielding effect of MiniPIX chassis can also be observed. For low-energy accelerated protons, this means that at high angles they approach their Bragg peak exactly in the active volume. By per-cluster analysis and spectral response of data acquired with Timepix3 detector single particle deposited energy can be observed together with the whole sensor spectral sensitivity, its energy range, as well as homogeneity of the 4H-SiC sensor.

The high granularity of Timepix detectors and their high-resolution spectral tracking allows one to measure the deposited energy in each pixel as well as the time of arrival of the collected charge. From the information acquired and processing of the cluster track, it is possible to calculate the track length of the particle through a sensor and subsequently to calculate LET of each individual particle in a wide range of energy and direction. The Figure 10 shows the normalised energy and LET distributions of selected proton clusters detected by L06-W0048 4H SiC detector at 0° (perpendicular) sensor proton beam irradiation at energies from 13 to 226 MeV. The proton beam must first pass the inactive 365.5 μm thick bulk 4H-SiC region which captures part of the proton energy. As the proton beam energy decreases, the proton deposited energy in sensor active region increases as the particle approaches its Bragg peak exactly in the radiation sensitive volume of the sensor. The filtration requirements for the proton clusters was set to clusters larger than four pixels that had energy deposited higher than 500, 300, 180, 90, and 40 keV at 13, 22, 31, 100, and 226 MeV proton beam energy, respectively. The upper energy cut-off value was set to 4000 keV for all distributions.

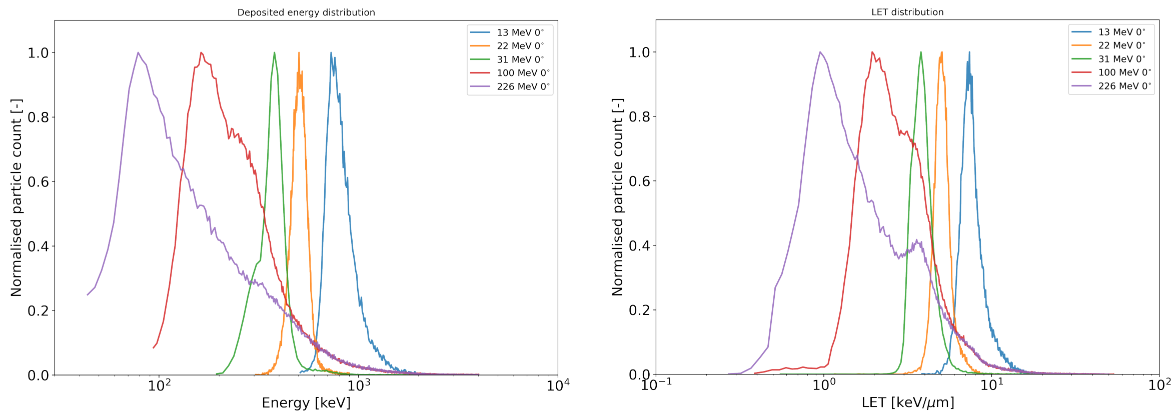

Figure 10: Deposited energy (left) and LET (right) spectra for protons of different energy. Measured by L06-W0048 4H-SiC Timepix3 placed perpendicular to the incident beam axis. A filter was applied to separate and analyse protons.

6.2 Response to energetic electrons in 5 - 8 MeV energy range

The behaviour of the electrons that pass through the sensor depend mainly on the energy, however, the primary mode of interaction is ionisation and scattering. As an electron passes through a matter volume, it ionises atoms by ejecting mainly valence electrons while simultaneously transmitting part of its energy. This process repeats in multiple cascade ionizations until the energy of the primary electron is less than that required for further ionisation. By visualising electrons passing through sensor of hybrid pixel detector, it can be observed that the particle track morphology is extensively curvy as the electron passes through the material. Due to a high number of collisions of electrons passing through matter, it can be observed that the energy distribution is skewed to the right, obtaining a high-energy tail, which is described by the Landau distribution. The amount of skewness depends on the sensor thickness and increases with the active volume. The most probable value in the asymmetric Landau distribution is the maximum value, while the average value is much more complicated to determine.

The SI-GaAs 350 μm thick sensor on Timepix ASIC operated in Time-over-Threshold mode was placed for in-beam measurement at a different angles of beam incidence to obtain rotation scan from 0° (perpendicular) to 87° (almost parallel with beam) angle of beam irradiation with respect to the sensor normal. The sensor irradiation is performed from the back side due to the fact that path required by a particle to reach active sensor volume is lower than from the front side irradiation considering the high-Z inactive volume above the active volume. The SI-GaAs 350 μm thick sensor suffers from a pixel cross-talk at high bias voltage and recommended bias value for optimal and stable performance is 60 V. During perpendicular irradiation at 0° angle with 5 MeV electron beam energy a bias scan was performed from 30 V to 110 V with a step of 10 V (corresponds to an increase of 7 μm of active thickness). In correlation with the change in bias, the active volume thickness of SI-GaAs also changes from 45 μm at 30 V to 101 μm at 110 V. The electron range in GaAs is 4.78 mm and 7.77 mm for 5 and 8 MeV electron beam energy, respectively.

The high-Z material advantage also lies in its stopping power of charged particles, however, in case of the SI-GaAs prototype grouped together with its only partial depletion results in a bulk of material 256 μm thick (at 100 V bias) that sits above the active volume and affects not only low-energy photon detection but detection of charged particles as well. A part of the impinging charged particle energy is deposited in the inactive volume and only a part of the particle energy is deposited and resolved in

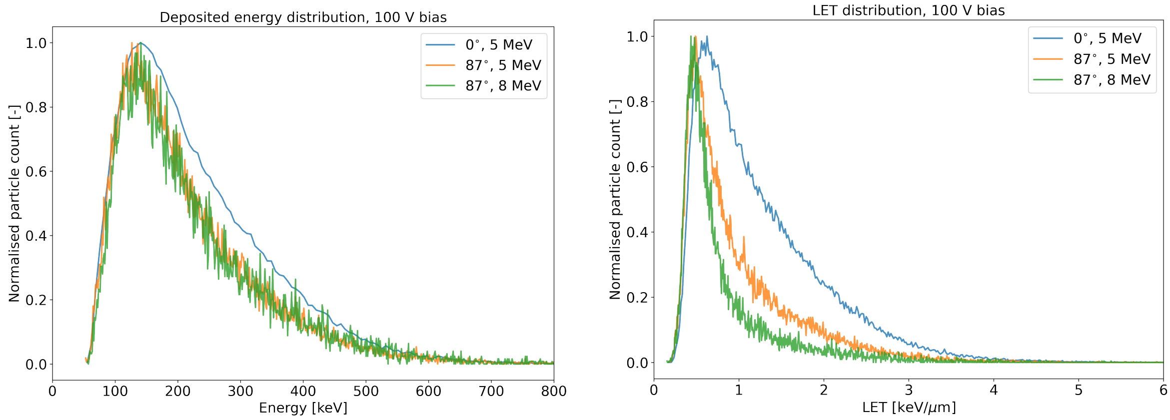

Figure 11: Normalised distribution of deposited energy and LET of events detected during 5 and 8 MeV electron irradiation of SI-GaAs 350 μm thick sensor on Timepix with FitPIX readout operated with 100 V bias. In this comparison distributions at 0° and 87° angle are demonstrated.

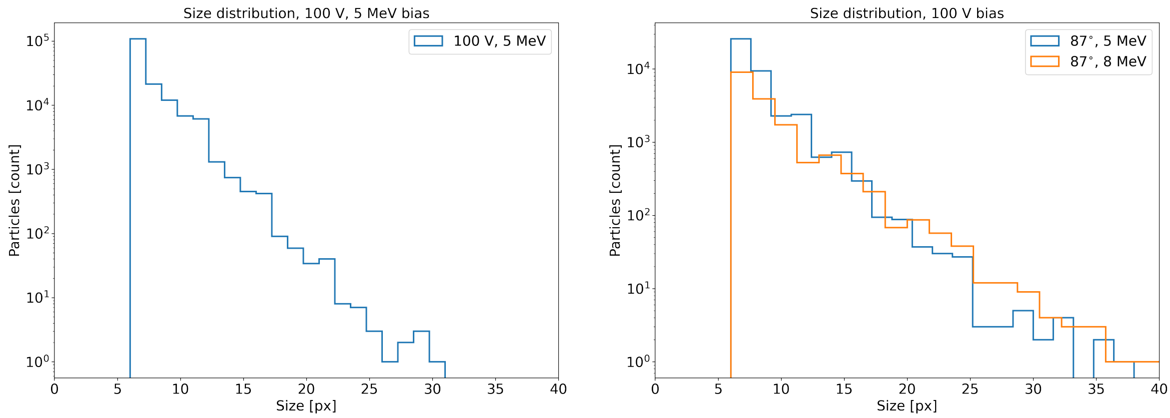

Figure 12: The distribution of cluster size of events detected during 5 and 8 MeV electron irradiation of SI-GaAs 350 μm thick sensor on Timepix with FitPIX readout. In this comparison distributions at 0° and 87° angle are demonstrated.

the active sensor volume. The deposited energy of detected charged particle also affects its calculated spectral parameters as well as the cluster morphology. As a result of limited thin active volume, the difference between particle group types is less pronounced with a large overlay. The same trouble occurs in thin 4H-SiC sensor with 65 μm active volume thickness. Only a selected few filter parameters are possible for confident use of specific particle type selection and filtration.

To effectively filter only desired particles, in this case charged electrons, a constraints were set to cluster energy and size. On top of these parameters an approach was used to utilize cluster skeleton in filtration process and limit cluster dataset to events that contain only two end/entry points. The normalised energy distribution and LET of filtered electrons is shown in Figure 11 for measurements acquired at 100 V bias, 0° and 87° angle of 5 and 8 MeV electron beam incidence. With regards to the deposited energy shown in Figure 11 (left) both distributions present identical results, while in the LET distribution (right) the main difference between the 5 and 8 MeV measurements is in the slower decaying tail at 5 MeV irradiation. With lower angle of beam incidence, the tail decay is slower from high angles near parallel to perpendicular. The difference of both 5 and 8 MeV energy electron beam irradiation can be seen in Figure 12 on a distribution of cluster size of filtered electrons where by tilting the sensor from 0° (perpendicular irradiation) to higher angle, here 87° is used, the distribution shifts to higher cluster size values.

6.3 Response to neutrons - 0.3 - 17.5 MeV energy range

The fast-neutron measurements at Van de Graaff accelerator were performed with monoenergetic neutrons in wide energy range from 0.3 to 17.5 MeV. For the purpose of new radiation-hard sensor characterisation both 4H-SiC sensors were used, L06-W0048 and L07-W0048, together with D05-W0037 Si sensor that was applied with a polyethylene and ^{6}LiF conversion layer for fast- and thermal-neutron conversion, respectively, and fixed with kapton tape. The position where each respective neutron conversion material is located on top of the sensor pixel matrix is graphically shown in Figure 13 (left). Both 4H-SiC sensors with Timepix3 ASIC were operated at 200 V bias voltage resulting in a 65 μm thick active region. Neutron irradiation causes a high radiation damage to materials and although the 4H-SiC offers only a limited active sensor volume, it is an ideal material for sensor manufacture intended for use in radiation-harsh environments since the SiC can withstand 1000-times the radiation damage of Si while simultaneously performing without any compromise in energy resolution. The 500 μm thick Si sensor with Timepix3 ASIC was operated at 80 V bias that was chosen to address the high-energy saturation and distortion [37] that is present in detection of heavy charged particles that occur in neutron irradiation measurements. The choice of lower bias voltage results in a fully depleted sensor while simultaneously causing a slower charge collection leading to charge cloud spreading over multiple pixels preventing excessive energy resolution distortion.

A high number of high-energy events, detected as a result of an increased probability of neutron interaction with each respective conversion layer, is registered in the position and in the close vicinity of the place where they are applied on the sensor. These regions can be expected to be pronounced by increased deposited energy also with respect to the neutron energy. The ^{6}LiF conversion layer provides an advantage in neutron energies below 1 MeV, while the polyethylene layer effect is the most useful in mid-range energies at units of MeV. At high neutron energies, the interaction with the Si and C atoms takes over and the high-energy events are registered thorough the whole sensor without any significant correlation with the location of conversion layers.

On top of the interactions with the conversion layers, the neutrons can also interact with lattice Si atoms as well as with C atoms in 4H-SiC sensors by elastic scattering, radiative capture or other nuclear reaction limited by their respective threshold energy value. These interactions occur regardless of the position within the sensor at a given energy threshold values and therefore they are detected thorough the whole sensor matrix and its volume. The detector granularity coupled with the spectral tracking of individual particles detected by the detectors allows to effectively discriminate other background events induced by the neutrons so that only high-energy events are filtered.

In the evaluation of the acquired data, namely in detected light and heavy ions, an edge effect needs to be addressed that affects all generated outputs. In the neutron interactions resulting in generation of proton, deuteron or alpha particle, based on the point of interaction, their energy and direction, the generated particle energy may not be fully deposited in the active sensor volume when the interaction takes place on the sides or edges of the sensor and the particle escapes its volume. On top of these events, in 4H-SiC the interaction can also take place in 365.5 μm thick inactive bulk layer, resulting in a loss of particle energy before reaching the 65 μm thick active sensor volume.

At high neutron energies that were used in these measurements, 15.5 and 17.5 MeV, the elastic neutron interaction remains prevalent thorough the whole pixel matrix. High-energy heavy charged particles are detected thorough the whole sensor and correspond to (n,α), (n,p), and (n,d) interactions

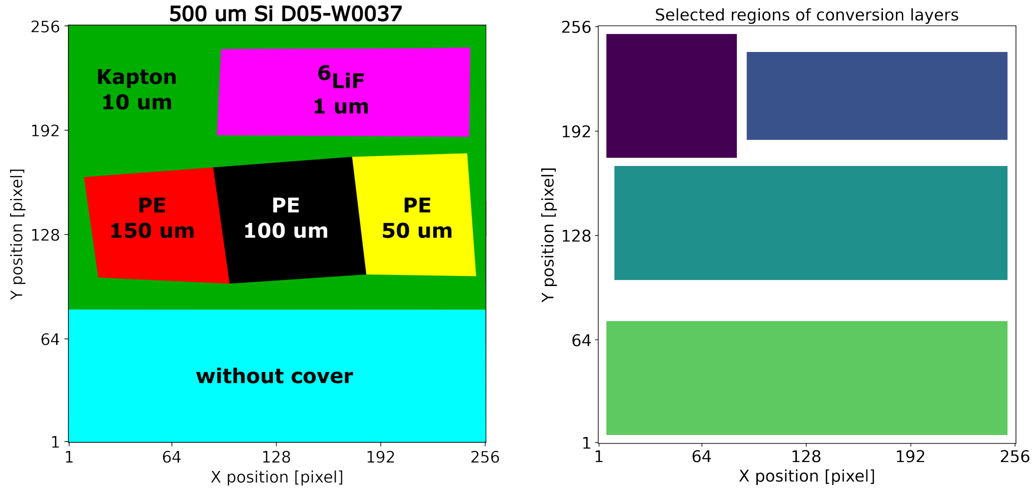

Figure 13: Regions of Timepix3 detector with 500 μm thick Si sensor used for neutron detection with conversion layers applied.

with lattice atoms.

All sensors used in neutron irradiation measurements are subjected to mixed radiation field components consisting not only heavy-charged particles arising from neutron interaction with the sensor, but also to electrons and photons. In order to quantify the effect of neutron interaction at different neutron energies it is required to filter high-energy events caused by heavy-charged particles detected in the sensors. For this purpose cluster parameter specific filtration can be employed.

For a precise approach of conversion layer evaluation, in the position of each respective region of the Si sensor, a sub-region was selected to specifically analyse only events with centroid within its borders. This is illustrated in Figure 13 with Si sensor regions (left) and their respective sub-region used in analysis (right). The acquired filtration results are also compared with the 4H-SiC sensors where the whole pixel matrix was analysed. In case of all three detectors, to mitigate the parasitic edge effect, events with centroid within 5-pixel border region are discriminated from the analysis. An illustration of filtered high-energy clusters in each respective region of 500 μm thick Si sensor in 4 MeV neutron measurement is shown in Figure 15.

In Table 2 the number of filtered events per second per cm^2 is listed as calculated for each neutron energy measurement and each region of Si as well as the 4H-SiC L06 and L07 sensors.

During the 15.5 MeV measurement, all sensors detected the highest number of high-energy events thorough the whole pixel matrix. The neutron interactions with the Si and C atoms take over and the effect of conversion layers decreases as can be seen in the difference of the filtered high-energy events beneath polyethylene layer with 187.3961 events/s/cm^2 and region of Si sensor without any covering layer with 152.6564 events/s/cm^2. Although the 4H-SiC sensors operated at 200 V bias offer only 65 μm thick active sensor region and as such are prone to edge effects described in the previous sections, their number of detected high-energy clusters is 64.5565 and 65.6839 events/s/cm^2 for L06 and L07 sensor, respectively.

With an increase of the neutron energy from 15.5 to 17.5 MeV the number of neutron interactions with Si and C atoms resulting in high-energy clusters drops significantly and therefore the number of events is in Si in range from 29.5706 (without cover) to 35.8909 events/s/cm^2 (polyethylene). In 4H-SiC this number is 10.604 and 8.273 events/s/cm^2 for L06 and L07, respectively.

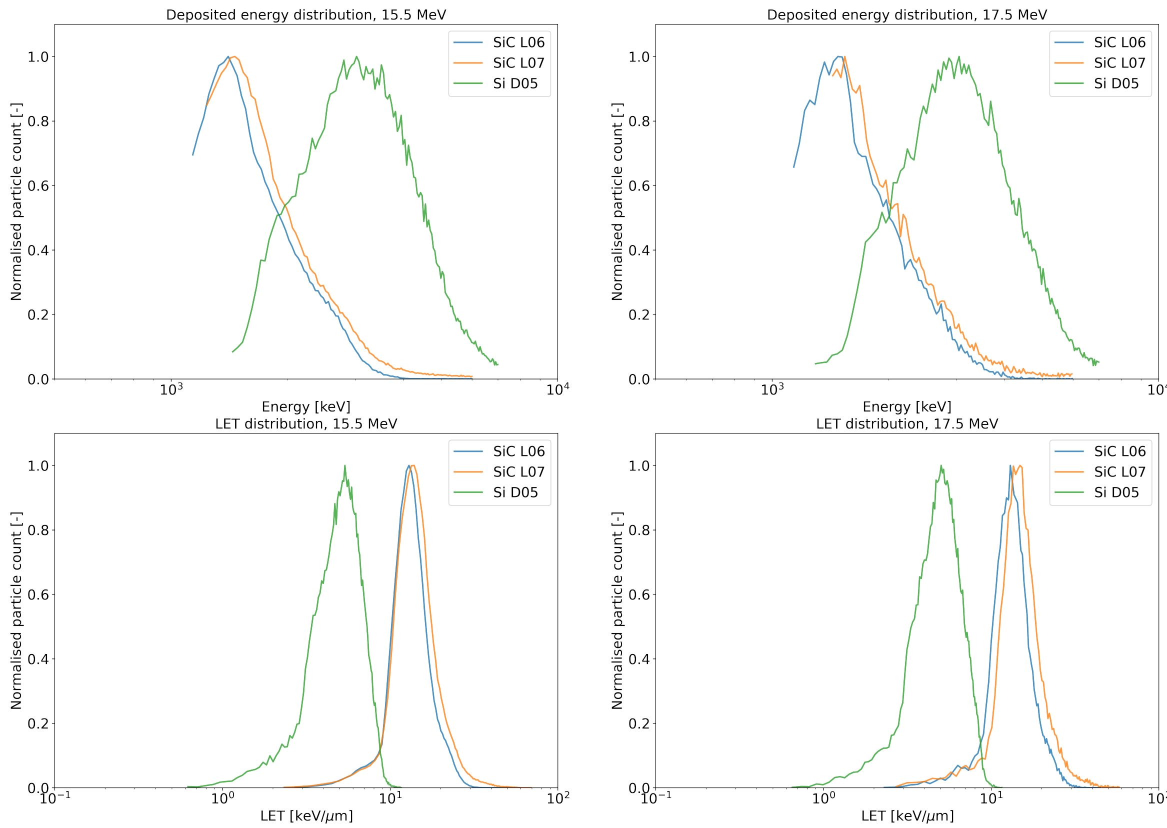

Figure 14: Deposited energy by high-energy clusters filtered from data acquired using Timepix3 detector with 500 μm thick Si and 65 μm 4H-SiC sensor during 17.5 MeV neutron irradiation.

Energy	^{6}LiF	PE	Kapton	Without cover	L06 4H-SiC	L07 4H-SiC
[MeV]	Filtered events flux [events/s/cm^2]					
0.3	4.7080	0.0019	0.0011	0.0135	0.0003	0.0017
0.5	5.2541	0.0012	0.0022	0.0118	-	0.0022
0.77	1.9473	0.0017	0.0028	0.0096	-	0.0024
1	0.0006	0.0009	0.0026	0.0003	0.0002	0.0034
3.3	1.8389	2.1035	1.9292	0.1599	0.0206	0.0253
4	15.1928	29.6227	14.8254	1.3697	0.2255	0.3363
5	15.5089	37.6416	14.9793	1.9645	0.3601	1.0460
15.5	170.7476	187.3961	173.3920	152.6564	64.5565	65.6839
17.5	35.5142	35.8909	35.8147	29.5706	10.6040	8.2730

Table 2: Neutron interaction analysis results with 500 μm thick Si sensor with conversion layers and 65 μm thick 4H-SiC sensors.

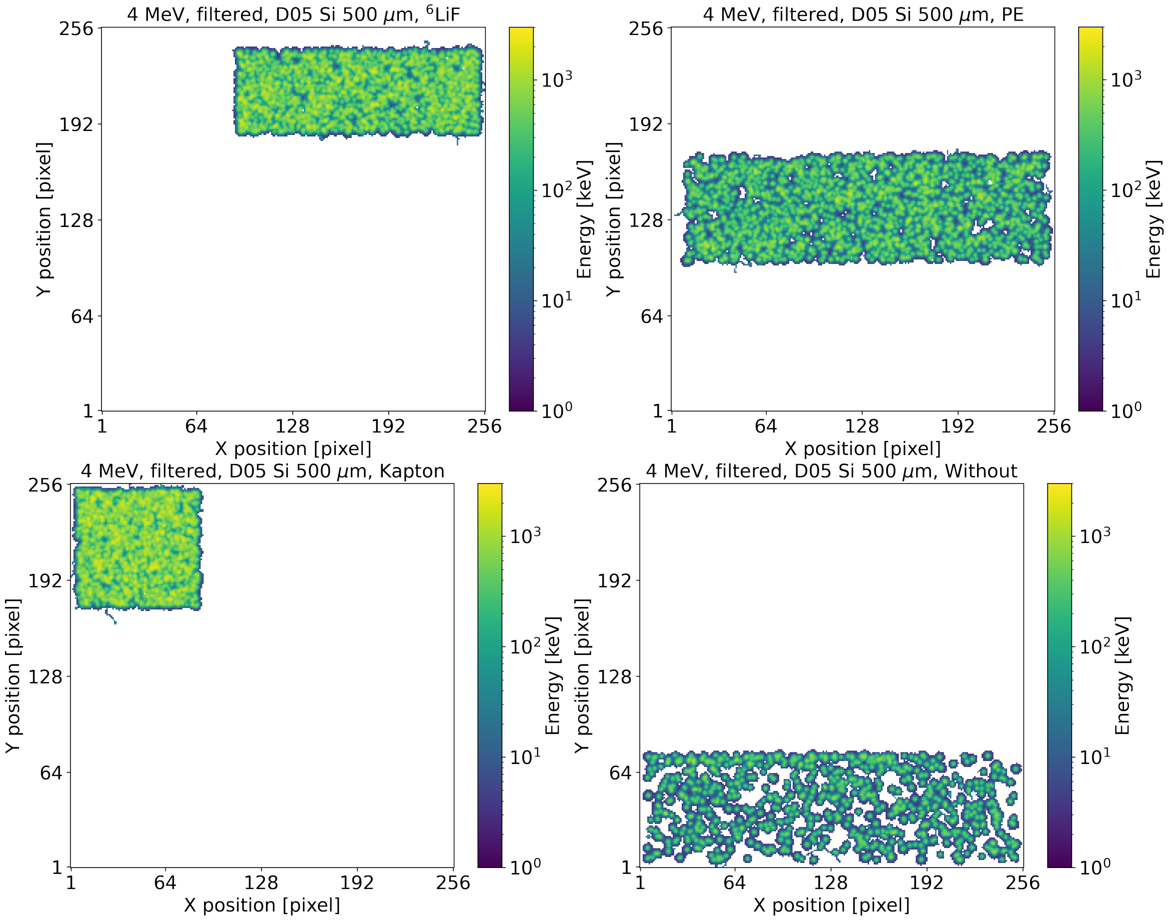

Figure 15: Illustration of filtered clusters in selected regions of 500 μm thick Si sensor at 4 MeV neutron measurement.

7 Contribution to the research field

The sensor semiconducting materials which I analysed thorough the thesis were Si, GaAs:Cr, SI-GaAs, CdTe and 4H-SiC; each with its respective variable thickness. Both SI-GaAs and epitaxially grown 4H-SiC sensors were prepared at the Institute of Electrical Engineering of the Slovak Academy of Sciences in Bratislava. The SI-GaAs, GaAs:Cr, and 4H-SiC sensor materials are regarded as radiation hard materials that can withstand higher radiation doses without significant performance deterioration. The advantage of the 4H-SiC lies also in its high thermal stability and radiation hardness while maintaining a high energy resolution comparable with commercially available and widely used Si sensors. The contribution of this thesis lies in following general remarks:

1. **Characterisation, comparison and performance analysis of newly developed SI-GaAs and 4H-SiC sensors for Timepix/2/3 hybrid pixel detectors** – experiments were performed using standard laboratory isotopes (laboratory of Institute of Nuclear and Physical Engineering) as well as energetic electrons, protons and fast-neutrons. Different sensor materials were investigated (Si, GaAs:Cr, SI-GaAs, CdTe, 4H-SiC) and compared with regard to their performance, charge-sharing effects, homogeneity and signal response. Accelerator facilities that were used in obtaining data for conducting this thesis contents and analyses:

- Electron cyclotron Microtron MT-25, Czech Academy of Sciences in Prague, electron energy range 5 - 8 MeV.
- Light ion cyclotron U-120M, Czech Academy of Sciences in Řež near Prague, proton energy range 8 - 31 MeV, ^{3}He ion energy range up to 38 MeV.
- Proton cyclotron C-235, Institute for Nuclear Physics, Cyclotron Centre Bronowice, Polish Academy of Sciences in Krakow, proton energy range 70 - 225 MeV.
- Proton cyclotron Proteus-235, Proton Therapy Center, Prague, proton energy range 100 - 226 MeV.
- Electrostatic Van de Graaff accelerator, Institute of Experimental and Applied Physics, Czech Technical University in Prague, fast-neutron energy range 0.3 - 17.5 MeV.

2. **Development of a complex data analysis workflow for spectral particle tracking of individual events** – data processing workflow aimed at optimized and automated decomposition, separation and analysis of individual events (clusters) detected by the hybrid pixel detectors using a range of radiation sources. Thorough investigation of each individual cluster event via calculation of spectral and morphological parameters characteristic for each ionizing particle-type group based on their interaction with each respective sensor material. Cluster skeletonization process developed and incorporated into the cluster event analysis for additional possibility of discovery and separation of rare events in large data volumes.

3. **Development of a filtration method for decomposition of mixed radiation fields** – automated analysis of fully described volumes of spectral and morphological cluster event data allowing for decomposition of mixed radiation fields obtained at various experiments into their respective experiment-specific components. This approach allows for an effective discrimination of undesirable background events and secondary radiation components in analyses of detector data obtained in a radiation-harsh environments. This aims for use of this approach in future utilization of radiation-hard SI-GaAs, GaAs:Cr and 4H-SiC sensors on Timepix/2/3 chip for applications such as accelerator beam monitoring, hadron therapy, cosmic weather research, etc. that pose a difficult challenge for commercially available materials such as Si and CdTe. The mixed radiation field decomposition has been successfully demonstrated in a published articles as well as in a number of experiments in this thesis which utilize mixed radiation fields at different accelerator facilities.

8 Summary

Thesis devotes to the development and characterisation of new semiconductor sensors for hybrid pixel detectors Timepix which are extensively used in applications of radiation detection and spectral analysis as well as in imaging applications utilizing X-rays, neutrons and high-energy charged particles. The work focuses on sensors made from radiation-hard materials GaAs (gallium arsenide) and 4H-SiC (hexagonal silicon carbide). These sensors have been implemented for Timepix readout electronics. Such hybrid pixel detectors can be used to analyse different types of radiation under laboratory conditions and also in particle accelerators producing high-intensity fields of high-energy electrons, protons and neutrons. The experimental data were processed at the level of individual detected events. Results are compared with existing available Timepix detectors with Si (silicon) and CdTe (cadmium telluride) sensors.

9 Zhrnutie

Práca sa venuje vývoju a charakterizácii nových polovodičových senzorov určených pre hybridné pixelové Timepix detektory využívané v oblastiach detekcie ionizujúceho žiarenia a spektrálnej analýzy, ako aj v zobrazovacích aplikáciách s využitím roentgenového žiarenia, neutrónov a vysokoenergetických nabitých častíc. Práca sa zameriava na senzory vyrobené z radiačne odolných materiálov, medzi ktoré patrí GaAs (arzenid gália) a 4H-SiC (hexagonálny karbid kremíka). Tieto senzory boli optimalizované pre vyčítavací obvod typu Timepix. S takýmito hybridnými pixelovými detektormi boli analyzované rôzne typy žiarenia v laboratórnych podmienkach ako aj v urýchľovačoch generujúcich vysokoenergetické elektróny, protóny a neutróny. Experimentálne získané dáta boli spracované na úrovni jednotlivých detegovaných udalostí a porovnané s komerčne dostupnými hybridnými pixelovými detektormi s Si (kremíkovými) a CdTe (telurid kadmia) senzormi.

10 References

[1] R. Ballabriga and et al. Asic developments for radiation imaging applications: The medipix and timepix family. *Nucl. Instrum. Methods Phys. Res. Sec. A: Accelerators, Spectrometers, Detectors and Associated Equipment*, 878:10–23, 2018.

[2] R. Ballabriga and et al. Photon counting detectors for x-ray imaging with emphasis on ct. *IEEE Transactions on Radiation and Plasma Medical Sciences*, 5(4):422–440, 2021.

[3] P. Stasica and et al. Single proton let characterization with timepix and artificial intelligence for proton therapy treatment planning. *Physics in Medicine & Biology*, 68:104001, 2023.

[4] C. Oancea and et al. Stray radiation produced in flash electron beams characterized by the minipix timepix3 flex detector. *Journal of Istrumentation*, 17:C01003, 2022.

[5] C. Oancea and et al. Out-of-field measurements and simulations of a proton pencil beam in wide range of dose rates with timepix3: Dose rate, flux and let. *Physica Medica*, 106:102529, 2023.

[6] St. Gohl and et al. A miniaturized radiation monitor for continuous dosimetry and particle identification in space. *IOP Publishing*, 7:2022, C01066.

[7] C. Schwarz and et al. X-ray imaging using a hybrid photon counting gaas pixel detector. *Nucl. Instrum. Methods Phys. Res. Sec. B - Proceedings Supplements*, 78(1):491–496, 1999. Advanced Technology and Particle Physics.

[8] E. Fröjdh and et al. Electron detection with cdte and gaas sensors using the charge integrating hybrid pixel detector jungfrau. *Journal of Instrumentation*, 17(01):C01020, jan 2022.

[9] D. Kubanda and et al. Performance of bulk semi-insulating gaas-based sensors with different pixel sizes for timepix radiation camera. In *2018 12th International Conference on Advanced Semiconductor Devices and Microsystems (ASDAM)*, pages 1–4, 2018.

[10] B. Zatko and et al. Imaging performance of a timepix detector based on semi-insulating gaas. *Journal of Instrumentation*, 13(01):C01034, jan 2018.

[11] B. Zatko and et al. Study of the contrast resolution of timepix detector with a semi-insulating gaas sensor. *Journal of Instrumentation*, 15(04):C04004, apr 2020.

[12] L. Tlustos and et al. Characterisation of a gaas(cr) medipix2 hybrid pixel detector. *Nucl. Instrum. Methods Phys. Res. Sec. A: Accelerators, Spectrometers, Detectors and Associated Equipment*, 633, 05 2011.

[13] J. M. Rafi and et al. Electron, neutron, and proton irradiation effects on sic radiation detectors. *IEEE Transactions on Nuclear Science*, 67(12):2481–2489, 2020.

[14] X. Llopart and et al. Timepix, a 65k programmable pixel readout chip for arrival time, energy and/or photon counting measurements. *Nucl. Instrum. Methods Phys. Res. Sec. A: Accelerators, Spectrometers, Detectors and Associated Equipment*, 581(1):485–494, 2007. VCI 2007.

[15] L. Marek and et al. Data processing engine (dpe): data analysis tool for particle tracking and mixed radiation field characterization with pixel detectors timepix, apr 2024.

[16] Introducing a 5mm CdTe Compton Camera with Timepix3 Technology. https://indico.cern.ch/event/1343953/contributions/5687419/. Contribution at the 24th International Workshops on Radiation Imaging Detectors.

[17] S. N. Ahmed. *Physics and engineering of radiation detection; 2nd ed.* Elsevier, Amsterdam, 2014.

[18] D. Maneuski and et al. Imaging and spectroscopic performance studies of pixelated cdte timepix detector. *Journal of Instrumentation*, 7(01):C01038, jan 2012.

[19] J. Breibach and et al. Development of a bump bonding interconnect technology for gaas pixel detectors. *Nucl. Instrum. Methods Phys. Res. Sec. A: Accelerators, Spectrometers, Detectors and Associated Equipment*, 470(3):576–582, 2001.

[20] L. Tlustos and et al. Characterisation of an epitaxial gaas/medipix2 detector using fluorescence photons. *Nucl. Instrum. Methods Phys. Res. Sec. A: Accelerators, Spectrometers, Detectors and Associated Equipment*, 591(1):42–45, 2008. Radiation Imaging Detectors 2007.

[21] A. Sagatova and et al. From single gaas detector to sensor for radiation imaging camera. *Applied Surface Science*, 461:3–9, 2018. 5th Progress in Applied Surface, Interface and Thin Film Science and Solar Renewable Energy News.

[22] B. Zatko and et al. First tests of timepix detectors based on semi-insulating gaas matrix of different pixel size. *Journal of Instrumentation*, 13(02):C02013, feb 2018.

[23] A. V. Tyazhev and et al. Gaas radiation imaging detectors with an active layer thickness up to 1mm. *Nucl. Instrum. Methods Phys. Res. Sec. A: Accelerators, Spectrometers, Detectors and Associated Equipment*, 509(1):34–39, 2003. Proceedings of the 4th Internatonal Workshop on Radiation Imaging Detectors.

[24] M. C. Veale and et al. Chromium compensated gallium arsenide detectors for x-ray and gamma-ray spectroscopic imaging. *Nucl. Instrum. Methods Phys. Res. Sec. A: Accelerators, Spectrometers, Detectors and Associated Equipment*, 752:6–14, 2014.

[25] P. Zambon and et al. Spectral and dqe performance of 300 μm and 500 μm thick gaas:cr x-ray photon counting detectors for imaging applications. *Nucl. Instrum. Methods Phys. Res. Sec. A: Accelerators, Spectrometers, Detectors and Associated Equipment*, 992:165046, 2021.

[26] G. Bertuccio and et al. Advances in silicon carbide x-ray detectors. *Nucl. Instrum. Methods Phys. Res. Sec. A: Accelerators, Spectrometers, Detectors and Associated Equipment*, 652(1):193–196, 2011. Symposium on Radiation Measurements and Applications (SORMA) XII 2010.

[27] G. Bertuccio and et al. Silicon carbide for high resolution x-ray detectors operating up to 100°c. *Nucl. Instrum. Methods Phys. Res. Sec. A: Accelerators, Spectrometers, Detectors and Associated Equipment*, 522(3):413–419, 2004.

[28] F. Nava and et al. Silicon carbide and its use as a radiation detector material. *Measurement Science and Technology*, 19(10):102001, aug 2008.

[29] J. M. Rafi and et al. Electron, neutron, and proton irradiation effects on sic radiation detectors. *IEEE Transactions on Nuclear Science*, 67(12):2481–2489, 2020.

[30] B. Zatko and et al. From a single silicon carbide detector to pixelated structure for radiation imaging camera. *Journal of Instrumentation*, 17(12):C12005, dec 2022.

[31] J. Jakubek. Precise energy calibration of pixel detector working in time-over-threshold mode. *Nucl. Instrum. Methods Phys. Res. Sec. A: Accelerators, Spectrometers, Detectors and Associated Equipment*, 633:S262–S266, 2011.

[32] A. Sagatova and et al. Electrical properties study of the 4H-SiC detectors based on thick epitaxial layer. *AIP Conference Proceedings*, 3054(1):050011, 2024.

[33] A. Novak and et al. Spectral tracking of proton beams by the timepix3 detector with gaas, cdte and si sensors. *Journal of Instrumentation*, 18:C01022, 2023.

[34] C. Granja and et al. Resolving power of pixel detector timepix for wide-range electron, proton and ion detection. *Nucl. Instrum. Methods Phys. Res. Sec. A: Accelerators, Spectrometers, Detectors and Associated Equipment*, 908:60–71, 2018.

[35] C. Granja and et al. Spectral and directional sensitive composition characterization of mixed-radiation fields with the miniaturized radiation camera minipix, timepix2. *Journal of Instrumentation*, 17:C11014, 2022.

[36] S. van derWalt and et al. scikit-image: Image processing in python. *PeerJ 2:e453*, 2014.

[37] M. Sommer and et al. High-energy per-pixel calibration of timepix pixel detector with laboratory alpha source. *Nuclear Instruments and Methods in Physics Research Section A: Accelerators, Spectrometers, Detectors and Associated Equipment*, 1022:165957, 2022.

11 Appendix A - List of author's published articles

[**A1**] A. ŠAGÁTOVÁ, B. ZAŤKO, E. KOVÁČOVÁ, A. NOVÁK, V. NEČAS, *Alfa spectrometry by radiation degraded semi-insulating GaAs detectors.* In Extended Abstract Book of Proceedings of SSSI 2020. Bratislava: Comenius University, 2020, 90–91. ISBN 978-80-223-5018-1.

[**A2**] A. ŠAGÁTOVÁ, E. KOVÁČOVÁ, A. NOVÁK, M. FÜLÖP, B. ZAŤKO, *Current-voltage characterization of GaAs detectors and their holders irradiated by high energy electrons.* Applied Surface Science, 2021, 552, 149474.

Cited in:

- S. J. Moloi, J. O. Bodunrin, *Characterisation of interface states of Al/p-Si Schottky diode by current–voltage and capacitance–voltage–frequency measurements.* J Mater Sci: Mater Electron, 2023, 34, 1712.

[**A3**] A. ŠAGÁTOVÁ, A. NOVÁK, E. KOVÁČOVÁ, P. BOHÁČEK, B. ZAŤKO, *Influence of SI GaAs base material on detector radiation hardness against high-energy electrons.* In Extended Abstract Book: of SURFINT-SREN VII, 2021, 67–68. ISBN 978-80-223-5296-3.

[**A4**] A. NOVÁK, A. ŠAGÁTOVÁ, B. ZAŤKO, C. GRANJA, D. CHVÁTIL, *Spectral Tracking in wide field-of-view of MeV electrons using Timepix detector with GaAs sensor.* In Proceedings of the 24th Conference of Doctoral Students (ELITECH 22), FEI STU, June 1st, 2022, Bratislava, Slovakia, ISBN 978-80-227-5192-6.

[**A5**] A. ŠAGÁTOVÁ, E. KOVÁČOVÁ, A. NOVÁK, V. NEČAS, B. ZAŤKO, *Alpha-spectrometry by radiation-degraded semi-insulating GaAs detectors.* In Materials Today: Proceedings 53. 2022, 293–298.

[**A6**] A. ŠAGÁTOVÁ, N. GÁL, A. NOVÁK, S. KOTOROVÁ, E. KOVÁČOVÁ, B. ZAŤKO, *GaAs radiation-degraded detectors: Gamma spectrometry at lowered temperatures.* In Journal of Instrumentation, 2022, JINST 17 C12018.

[**A7**] B. ZAŤKO, A. ŠAGÁTOVÁ, N. GÁL, A. NOVÁK, J. OSVALD, P. BOHÁČEK, Š. POLANSKY, J. JAKUBEK, E. KOVÁČOVÁ, *From a single silicon carbide detector to pixelated structure for radiation imaging camera.* In Journal of Instrumentation, 2022, JINST 17 C12005.

[**A8**] C. GRANJA, J. JAKUBEK, P. SOUKUP, M. JAKUBEK, D. TURECEK, L. MAREK, S. POLANSKY, J. GAJEWSKI, A. RUCINSKI, P. STASICA, M. RYDYGIER, A. NOVAK, D. POKLOP, *Spectral and directional sensitive composition characterization of mixed-radiation fields with the miniaturized radiation camera MiniPIX Timepix2.* In Journal of Instrumentation, 2022, JINST 17 C11014.

Cited in:

- T. Ari-Izumi, G. Takashi, I. Gheorghe, D. Filipescu, S. Hashimoto, S. Miyamoto, H. Utsunomiya, *Spatial profiles of collimated laser Compton-scattering γ-ray beams.* In Journal of Instrumentation, 2023, JINST 18 T06005.

- D. Filipescu, I. Gheorghe, S. Goriely, A. Tudora, K. Nishio, T. Ohtsuki, H. Wang, G. Fan, K. Stopani, F. Suzaki, K. Hirose, M. Inagaki, Y. Lui, T. Ari-izumi, S. Miyamoto, T. Otsuka, H. Utsunomiya, *Giant dipole resonance photofission and photoneutron reactions in U 238 and Th 232.* In Physical Review C, 2024, 109, 044602.

- D. Hladik, J. Jakubek, K. Sykorova, T. Cerna, D. Doubravova, M. Urban, S. Polansky, *Optimizing and characterizing the Timepix2 hybrid pixel detector: enhancing performance and precision for scientific and industrial applications.* In Journal of Instrumentation, 2024, JINST 19 C01007.

[**A9**] A. NOVÁK, A. ŠAGÁTOVÁ, B. ZAŤKO, *Energy Calibration of Timepix Detector with GaAs Sensor.* In AIP Conference Proceedings, 2023, 2778.

[**A10**] A. NOVÁK, C. GRANJA, A. ŠAGÁTOVÁ, C. OANCEA, V. ZACH, J. STURSA, *Spectral tracking of protons by the Timepix3 detector with GaAs, CdTe and Si sensors.* In Journal of Instrumentation, 2023, JINST 18 C01022.

Cited in:

- L. Marek, C. Granja, J. Jakubek, J. Ingerle, D. Turecek, M. Vuolo, C. Oancea, *Data Processing Engine (DPE): data analysis tool for particle tracking and mixed radiation field characterization with pixel detectors Timepix.* In Journal of Instrumentation, 2024, JINST 19 C04026.

- P. Stasica, H. Nguyen, C. Granja, R. Kopec, L. Marek, C. Oancea, L. Raczynski, A. Rucinski, M. Rydygier, K. Schubert, R. Schulte, J. Gajewski, *Single proton LET characterization with the Timepix detector and artificial intelligence for advanced proton therapy treatment planning.* In Physics in medicine and biology, 2023, 68.

- C. Balan, C. Granja, G. Mytsin, S. Shvidky, A. Molokanov, L. Marek, V. Chis, C. Oancea, *Particle Tracking, Recognition and LET Evaluation of Out-of-Field Proton Therapy Delivered to a Phantom with Implants.* In arXiv eprint, 2023, 2312.14304.

[**A11**] A. ŠAGÁTOVÁ, A. NOVÁK, E. KOVÁČOVÁ, O. RIABUKHIN, S. KOTOROVÁ, B. ZAŤKO, *Radiation-degraded Si GaAs detectors and their metallization.* In AIP Conference Proceedings, 2023, 2778.

[**A12**] A. NOVÁK, A. ŠAGÁTOVÁ, C. GRANJA, V. ZACH, J. STURSA, *Cluster Core-Halo Delay Study on MeV Proton Tracks in GaAs:Cr Sensor on Timepix3 Detector.* In Proceedings of the 25th Conference of Doctoral Students (ELITECH 23), FEI STU, May 31st, 2023, Bratislava, Slovakia, ISBN 978-80-227-5298-5.

[**A13**] A. NOVAK, C. GRANJA, A. SAGATOVA, J. JAKUBEK, B. ZATKO, V. VONDRACEK, M. ANDRLIK, V. ZACH, S. POLANSKY, A. RATHI, C. OANCEA, *Silicon Carbide Timepix3 detector for quantum-imaging detection and spectral tracking of charged particles in wide range of energy and field-of-view.* In Journal of Instrumentation, 2023, JINST 18 C11004.

[**A14**] A. NOVÁK, C. CARLOS, A. ŠAGÁTOVÁ, V. ZACH, J. STURSA, *A Simple Approach to MeV Proton Track Filtration and Analysis in Timepix3 Hybrid Pixel Detector with Si, CdTe and GaAs sensor.* In AIP Conference Proceedings, 2024, 3054.

[**A15**] B. ZATKO, E. KOVACOVA, N. KURUCOVA, A. NOVAK, A. SAGATOVA, *Imaging and spectrometric performance of SiC Timepix3 radiation camera.* In Journal of Instrumentation, 2024, JINST 19 C01003.

[**A16**] A. SAGATOVA, M. FULOP, A. NOVAK, B. VRBAN, J. LULEY, S. CERBA, I. BENKOVSKY, B. ZATKO, *Conversion of fast neutrons for neutron radiography with TPX2 detector.* In NUKLEONIKA 69(2), 2024, 135-140.

[**A17**] A. SAGATOVA, B. ZATKO, A. NOVAK, *Perspective SiC Sensor for Radiation Camera.* In Nuclear Physics News, 2024, 34(2), 27–30.